Temporally Resolving Synchronous Degenerate and Nondegenerate Two-Photon Absorption in 2D Semiconducting Monolayers

Qiannan Cui,*,† Yuanyuan Li,‡ Jianhua Chang,‡ Hui Zhao,¶ and Chunxiang Xu*,†

†*State Key Laboratory of Bioelectronics, School of Biological Science and Medical Engineering, Southeast University, Nanjing 210096, China*

‡*Jiangsu Key Laboratory of Meteorological Observation and Information Processing, Nanjing University of Information Science & Technology, Nanjing 210044, China*

¶*Department of Physics and Astronomy, The University of Kansas, Lawrence, Kansas 66045, United States*

E-mail: qiannan@seu.edu.cn; xcxseu@seu.edu.cn

Abstract

Degenerate and nondegenerate two-photon absorption (TPA) in WS_2 and $MoSe_2$ monolayers are synchronously induced and temporally resolved by femtosecond laser pump-probe. Differential transmission signals in the first 500 fs consist of negative and positive components, that originate from direct probe depletion via nondegenerate TPA and carrier accumulation via degenerate TPA, respectively. Temporal cross-correlation of pump and probe pulses allows us to fully decouple the ultrafast nondegenerate and degenerate TPA signals. Subsequently, degenerate and nondegenerate TPA coefficients are calculated as a function of pump irradiance. Under non-resonant pumping, 100 ± 10 cm/GW and 250 ± 25 cm/GW are obtained for degenerate and nondegenerate

TPA coefficients of monolayer WS_2, respectively, which both present linearly decreasing trends as increasing pump irradiances. However, under resonant pumping of $2p$ excitonic states in monolayer $MoSe_2$, degenerate TPA coefficients exponentially decrease from 800 to 80 cm/GW as increasing pump irradiances, due to the interplay between band-renormalization and band-filling effects, while nondegenerate TPA coefficient is about 650 ± 50 cm/GW. For comparison, a trilayer $MoSe_2$ is also investigated. These results set a foundation for precisely measuring TPA coefficients and actively controlling nonlinear excitonic dynamics via TPA in 2D semiconducting monolayers.

KEYWORDS: degenerate two-photon absorption, nondegenerate two-photon absorption, femtosecond laser pump-probe, transition metal dichalcogenide, two-dimensional monolayer

1. Introduction

Transition metal dichalcogenide (TMD) monolayers possess a sub-nanometer thickness and appealing optoelectronic properties, such as direct band gaps in the visible region[1] and superior luminescent performances,[2] facilitated by their large exciton binding energies.[3,4] Encouraged by their large linear optical-absorption coefficients, tremendous efforts have demonstrated that TMD monolayers are ideal semiconducting materials for applications in many fields, such as efficient solar cells,[5,6] nanolasers[7,8] and biomedical engineering.[9,10] Beyond the linear optical regime, extensive efforts in recent years have been devoted to investigating nonlinear optical responses of TMD monolayers up to the third-order. These studies provided valuable information of lattice structure,[11,12] nonlinear absorption coefficients,[13–19] fine structures of excitonic levels,[20–22] and realized subband photodetection,[23] tunable nonlinear optical response,[24,25] quantum coherence,[26–28] etc.

In general, third-order nonlinear optical performances of a material, such as saturable absorption (SA), third harmonic generation (THG) and four-wave mixing (FWM), are dom-

inated by its third-order susceptibility. Comparing with second-order nonlinear optical studies, it's more difficult to perform accurate measurements of third-order susceptibility of TMD monolayers with a lateral size of micrometer-scale. Taking advantage of giant peak intensity and spatiotemporal coherence of femtosecond lasers, several nonlinear optical spectroscopy techniques have been developed for 2D monolayers to study and quantify their third-order nonlinear optical properties. To obtain the real part of third-order susceptibility, femtosecond laser THG measurements have been carried out for graphene,[29,30] MoS_2,[31] ReS_2,[12] black phosphorus,[32,33] etc. In addition, to obtain the imaginary part of third-order susceptibility, which is proportional to two-photon absorption (TPA) coefficient, degenerate TPA Z-scan technique has been used for uniform films of TMDs grown by chemical vapor deposition (CVD).[17–19] Z-scan's simplicity of one-laser-beam setup has made it widely employed,[34] while it can suffer from low spatial resolution and limited temporal resolution.[35–37]

TPA is an elementary third-order nonlinear optical process involving simultaneous absorption of two photons of same (degenerate) or different (nondegenerate) energies by a medium. Degenerate and nondegenerate TPA usually dominate 2D semiconducting monolayers' performances when these materials serve as saturable absorber or gain medium in lasing applications. Inside a laser cavity where light is not monochromatic, degenerate and nondegenerate TPA can be co-existing, and temporally resolving them as well as measuring their coefficients are fundamentally essential. Besides high light intensity applications, nondegenerate TPA of 2D semiconducting monolayers are potentially important for subband photodetections involving extremely low light intensity. Previously, it has been demonstrated that performances of infrared detections with traditional semiconductors of wide band gap via nondegenerate TPA were comparable to or even better than that of commercial infrared detectors via one-photon absorption.[38–40] For instance, Fishman et al. have realized sensitive detection of weak mid-infrared radiation in GaN via nondegenerate TPA of a gated visible photon and an infrared photon,[39] facilitated by strongly enhanced nondegenerate TPA coefficients. Comparing with traditional semiconductors, intense excitonic resonances

of 2D semiconducting monolayers are expected to further enhance nondegenerate TPA coefficients, making them promising candidate of novel subband photodetectors. Their relatively wide range of excitonic resonances between the optical gap and electronic gap can also potentially lead to broadband performances of subband photodetection. In addition, intrinsic properties of 2D semiconducting monolayers, such as atomic thickness, superior mechanical flexibility and large in-plane anisotropy, provide complementary degrees of freedom that conventional semiconductors or systems can not achieve. Hence, experimental measurements of degenerate and nondegenerate TPA coefficients of 2D semiconducting monolayers will serve as a ubiquitous benchmark for both high and low light intensity applications.

Here we report a study of temporally resolving synchronous degenerate and nondegenerate TPA with femtosecond laser pump-probe in WS_2 and $MoSe_2$ monolayers. By tuning photon energies of pump and probe with respect to the optical band gap of the TMD monolayers, resonant and non-resonant pumping conditions were selectively applied. We found time-resolved differential transmission signals evolve from negative to positive within the first 500 fs, synchronously induced by nondegenerate and degenerate TPA, respectively, when the probe pulse is temporally scanned across the pump pulse. Moreover, we fully decoupled degenerate and nondegenerate TPA signals and calculated degenerate and nondegenerate TPA coefficients. Although nondegenerate TPA coefficients are larger by a few factors than degenerate TPA cases, excitonic resonance can significantly enhance degenerate TPA coefficients by one order of magnitude in monolayer $MoSe_2$. Such excitonic resonance enhancement can be rapidly switched off by increasing pump irradiance, due to the red shift of $2p$ excitonic level induced by band renormalization effect. These results are important for accurately measuring TPA coefficients and actively controlling excitonic dynamics via TPA in 2D semiconducting monolayers.

2. Experimental Section

Our samples are mechanically exfoliated from bulk crystals purchased from $2D\ Semiconductors$. Optical contrasts of these samples are recorded by a commercial optical microscope. Facilitated by PDMS stamps, these samples are then transferred to three different BK7 glass substrates, which are all about 0.48 mm thick. To confirm thicknesses of our samples, optical contrast analysis and photoluminescence (PL) measurements are performed. In PL measurements, samples are irradiated by a continuous-wave (CW) 405 nm laser, which is tightly focused on samples by an objective lens with a high numerical aperture. Reflected PL is collected by the same objective lens and sent to a spectrometer, before which a long-pass filter is deployed to eliminate 405 nm residual.

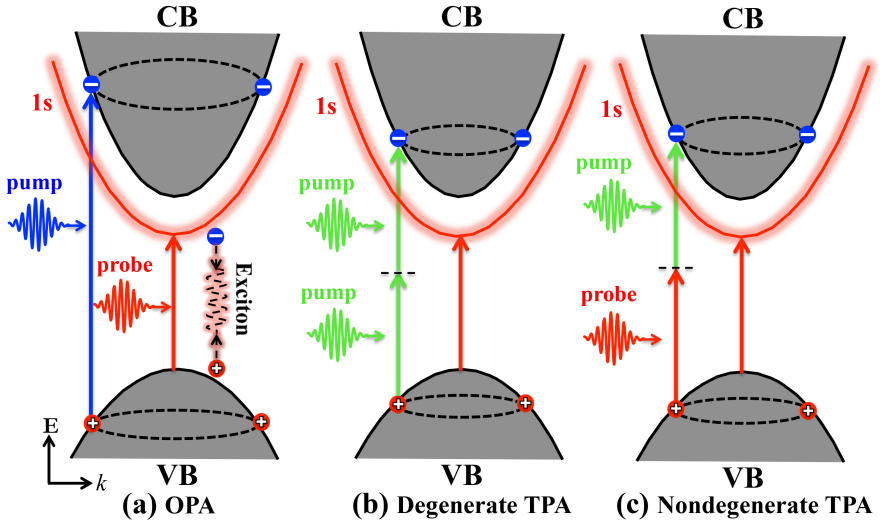

Figure 1: Photon energy of the probe is fixed at optical band gap of 2D monolayer E_x to detect exciton population around $1s$ excitonic state. (a) When photon energy of the pump is bigger than electronic band gap E_g, OPA is induced; When photon energy of the pump is between $0.5E_x$ and E_x, (b) Degenerate TPA and (c) Nondegenerate TPA are synchronously induced.

Degenerate and nondegenerate TPA in 2D semiconducting monolayers are synchronously induced and accurately measured by femtosecond laser pump-probe technique (see Supporting Information). A schematic illustration of our experimental technique is presented in Figure 1. When the photon energy of the pump pulse is higher than the electronic band gap

E_g, an electron can transit from valence band to conduction band by absorbing one pump photon in a one-photon absorption (OPA) process as shown in Figure 1(a). The photon energy of probe pulse is tuned to the optical band gap E_x, which is the energy difference between $1s$ level of A-exciton and the top of valence band, so that photoexcited excitons are monitored according to the transmission power change of probe going through the sample. By tuning the time delay between probe and pump pulses, temporal dynamics of injected carriers is measured. When the photon energy of pump pulse is between $0.5E_x$ and E_x, degenerate and nondegenerate TPA can occur synchronously. The transition of an electron can be induced by simultaneously absorbing two pump photons, as shown Figure 1(b), that is degenerate TPA. In the meantime, the transition of an electron can also be induced by simultaneously absorbing one pump photon and one probe photon, as shown Figure 1(c), that is nondegenerate TPA. When photon energy of the probe is still fixed at E_x, resolving degenerate and nondegenerate TPA processes rely on different observables of the probe. To be specific, for degenerate TPA measurement, the differential transmission of probe will be proportional to the injected carrier density; for nondegenerate TPA measurement, the differential transmission of probe will be corresponding to direct power depletion of probe.

3. Results and Discussion

To demonstrate our technique, we first carry out measurements on a monolayer WS_2 sample in ambient conditions. PL of the exfoliated monolayer WS_2 on a BK7 glass substrate presents an asymmetric shape with a peak of about 622 nm as shown in Figure 2(a), indicated by the red dashed line. The optical contrast of the monolayer region in green channel from the inset of Figure 2(a) is about 6 %. These results agree well with previous reports [41,42] and confirm the monolayer nature of our WS_2 sample. A time-resolved pump-probe setup with two pump arms and one probe arm, is constructed (see Supporting Information). 388 nm femtosecond laser pulse is deployed in one pump arm to induce OPA and 776 nm femtosecond laser pulse

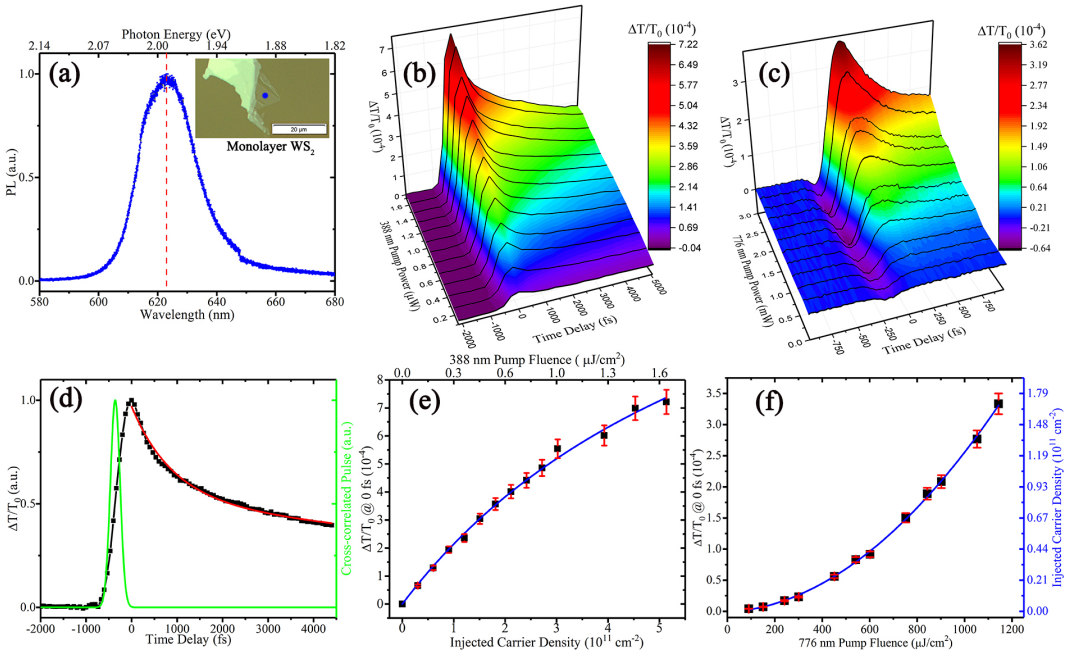

Figure 2: (a) PL spectrum (blue curve) of monolayer WS_2 with a peak of 622 nm (red dashed line). Inset is sample's optical microscope image, and the blue dot is laser focusing position. Temporal scans of differential transmission signals in (b) OPA measurements under various 388 nm pump powers (0.1-1.7 μW) and in (c) TPA measurements under various 776 nm pump powers (0.23-2.96 mW). Negative signals before 0 fs are induced by nondegenerate TPA of one pump photon and one probe photon. (d) An example of temporal scans in (b). The green curve is a Gaussian pulse with FWHM of 250 fs. The solid red line is a bi-exponential fitting, with a fast and slow decay time of 1 ps and 14 ps, respectively. (e) Differential transmission signals at 0 fs (black squares) as a function of injected carrier density via OPA. The solid blue line is a sublinear fitting. (f) Differential transmission signals at 0 fs (black squares) as a function of 776 nm pump fluence. The solid blue line is a quadratic fitting.

is sent to the other pump arm to induce TPA. A weak 620 nm femtosecond laser pulse serves as the probe. Considering exciton binding energy of about 320 meV [3] and optical band gap E_x = 2.0 eV, photon energy of 388 nm pump is higher by 870 meV than monolayer WS_2 electronic band gap. In this scenario, final states of electron transition via both OPA and TPA fall into continuum states in conduction band. Hence, we are applying non-resonant pumping conditions for monolayer WS_2 measurements. To study OPA of monolayer WS_2, the 776 nm pump arm is blocked. By tuning the time delay between the probe and pump pulses, temporal dynamics of transient absorption induced by OPA is monitored. Pump power dependence of temporal dynamics of injected carrier is illustrated in Figure 2(b). Temporal evolution of transient absorption has two stages: a rising part and a decay part. The rising part is carrier accumulation process of the pump sensed by differential transmission of probe, which can be described by a time integral of cross-correlation between pump and probe pulses. Assuming both pump and probe pulses are Gaussian in the time domain, we define the ending time of the rising part, that is the peak of positive signals, as 0 fs for the sake of simplicity in following discussions. The decay part can be fitted by a bi-exponential functions, corresponding to carrier thermalization and exciton recombination processes, which have been well discussed in previous reports. [43,44]

To establish a relationship between maximal carrier density injected by OPA and pump fluence, we assume each absorbed 388 nm photon only excite one pair of photocarrier, that is one electron and one hole, maximal carrier density N can be calculated by

$$N = \frac{F_{peak}}{h\nu}(1 - e^{-\alpha L}) = \frac{8ln2}{\pi}\frac{P(1 - e^{-\alpha L})}{h\nu f_{rep}\omega^2}, \quad (1)$$

where OPA pump power P = 1 μW, laser pulse repetition frequency f_{rep}=80.48 MHz and full width at half maximum (FWHM) of cross-correlated profile of pump and probe spots ω = 1.5 μm. Knowing the linear absorption coefficient $\alpha = 2.3 \times 10^8$ m^{-1}, [5,45] the thickness of monolayer WS_2 L = 0.75 nm, [46,47] and peak fluence of OPA pump $F_{peak} \approx 0.975$ $\mu J/cm^2$, it is straightforward to obtain the injected carrier density $N = 3.02 \times 10^{11}$ cm^{-2}. We can

estimate the 388 nm pump fluence of 1 μJ/cm^2 will lead to maximal injected carrier density of about 3.1 $\times$ 10^{11} cm^{-2}. Differential transmission of probe at 0 fs is plotted as a function of injected carrier density as shown in Figure 2(e), which indicates a sub-linear trend. This dependence can be fitted by a saturation model,[48]

$$\frac{\Delta T}{T_0} = A\frac{N}{N+N_0}, \tag{2}$$

where N_0 denotes the carrier density of saturation. From the fit indicated by the solid blue line, we have $A = 0.002$ and $N_0 = 7.4 \times 10^{11}$ cm^{-2}. Based on these analyses, a differential signal of $\frac{\Delta T}{T_0} = 1.0 \times 10^{-4}$ corresponds to an injected carrier density of about 0.560×10^{11} cm^{-2}.

Next, we investigate TPA in monolayer WS_2 with 776 nm pump and the other conditions are kept the same as OPA measurements with 388 nm pump. Pump power dependence of probe differential transmission at different time delays, is presented in Figure 3(c) with a set of negative dips observed before 0 fs. In this scenario, there are two different paths to realize the electron transition from valence band to conduction band. One is degenerate TPA while two 776 nm pump photons are simultaneously absorbed, and the other is nondegenerate TPA while one 776 nm pump photon and one 620 nm probe photon are simultaneously absorbed. Injected carrier density is a sum contribution of both nondegenerate TPA and degenerate TPA. However, it should be noticed that in our measurements the power of 620 nm probe is about three orders of magnitude smaller than powers of 776 nm pump. Assuming nondegenerate TPA coefficient is equal to degenerate TPA coefficient, the contribution of nondegenerate TPA to total carrier density will be approximately three-order of magnitude smaller than degenerate TPA contribution. Therefore, in our experiments, nondegenerate TPA contribution to total carrier density can be neglected. In Supporting Information, a detailed calculation is presented. To perform an accurate analysis of our TPA results, the differential transmission signals at 0 fs are plotted as a function of pump fluences in Figure 2(f). The solid blue line is a quadratic fitting, agreeing well with experimental data. This

further confirms that the differential transmission signal at 0 fs is mainly contributed by degenerate TPA.

To fully decouple the nondegenerate TPA components in the time domain, we take advantage of the temporal cross-correlation between pump and probe pulses. First of all, initial states in the valence band and final states in conduction band of electron transition via degenerate TPA should be the same as OPA case, because OPA pump originates from SHG of degenerate TPA pump. As a result, temporal dynamics of carrier injection and relaxation processes via degenerate TPA should be also the same as OPA case. Assuming both pump and probe pulses are Gaussian in the time domain, carrier injection via degenerate TPA before 0 fs is expected to behave exactly the same as the transient absorption of OPA showing a positive rising trend. This positive rising trend accounts for carrier accumulation in the time domain, and can be fitted by an integral of the temporal cross-correlation between pump and probe pulses. To estimate the temporal cross-correlation of pump and probe pulses in TPA measurements, we fit the rising part of OPA temporal dynamics of probe differential transmission before 0 fs in Figure 2(b). A fitting example is illustrated in Figure 2(d) when pump power is about 1 μW, indicating FWHM of cross-correlation between pump and probe pulses for OPA measurements is about 250 fs. Secondly, nondegenerate TPA directly points to irradiance depletion of 620 nm probe pulses, which will induce negative signals of probe differential transmission before 0 fs. The temporal evolution of negative dips in Figure 2(c) should be a negative convolution between pump and probe pulses. Therefore, probe differential transmission we have observed before 0 fs can be described by a negative Gaussian function plus an integral of positive Gaussian function, corresponding to probe irradiance depletion process caused by nondegenerate TPA and carrier accumulation process induced by degenerate TPA, respectively. Such unique features allow us to completely decouple the degenerate and nondegenerate TPA processes, both synchronously occurring before 0 fs.

In Figure 3(a), we present an example of the decoupling process, where the black squares are the observed data in Figure 2(c) when the 776 nm pump power is 2.96 mW (correspond-

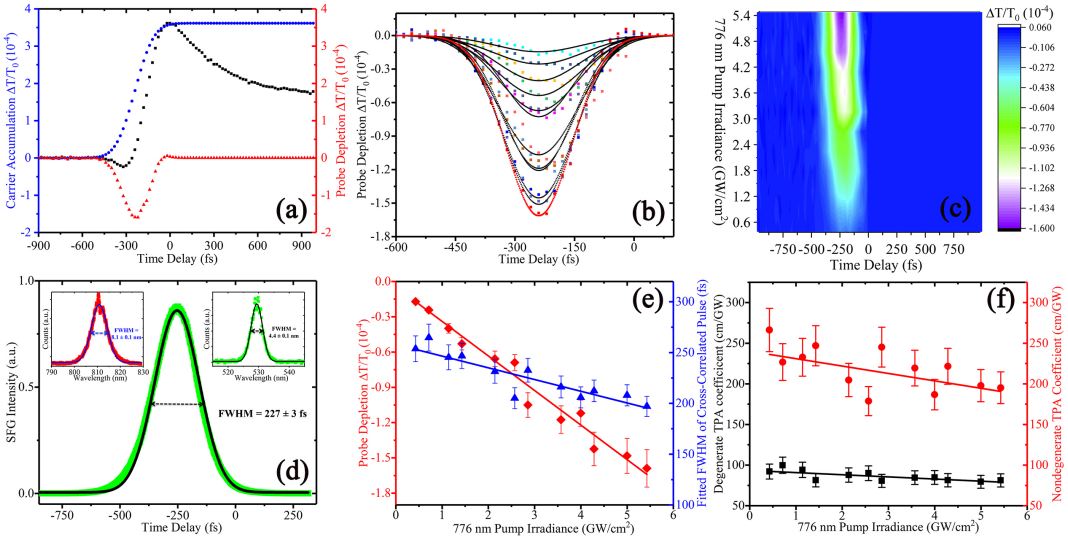

Figure 3: (a) An example of decoupling process when 766 nm pump power is 2.96 mW. Black squares are original data, and blue dots are degenerate TPA component obtained by integrating a Gaussian pulse with FWHM of 250 fs. Red triangles are obtained by subtracting blue from black. (b) Decoupled nondegenrate TPA components under 776 nm pump powers from 0.23 mW (top) to 2.96 mW (bottom). (c) 2D contour plotting of (b). (d) Temporal cross-correlation of pump and probe pulses by SFG of a BBO crystal. Insets are steady spectra of Ti: sapphire oscillator output (red suqares) and SFG (green squares). (e) Probe depletions at - 250 fs (red diamonds) induced by nondegenerate TPA as a function of 776 nm pump irradiance. Blue triangles are FWHM of fitted curves in (b). (f) Degenerate TPA coefficients (black squres) and nondegenerate TPA coefficients (red circles) under different 776 nm pump irradiances. Solid lines are linear fittings.

ing pump irradiance is 5.43 GW/cm^2). Blue circles, positive signals of carrier accumulation process, are fitted by a function of Gaussian integral, since we know that FWHM of the Gaussian function, that is temporal convolution of pump and probe pulses, is about 250 fs. Decoupled nondegenerate TPA signals, red triangles, are then obtained by subtracting the blue circles from the black squares. In this way, nondegenerate TPA signals under other pump irradiances can be decoupled. We emphasize that negative signals of nondegenerate TPA, indicated by red triangles in Figure 3(a), are fitted by appointing the directly observed peak position of probe differential transmission as the reference position. So it is straightforward and reasonable to define the peak position as zero delay (0 fs) instead of the valley position of fitted nondegenerate TPA signals to elaborate our decoupling process. In Figure 3(b), decoupled nondegenerate TPA signals under 776 nm pump powers from 0.23 mW (top) to 2.96 mW (bottom) are fitted by negative Gaussian functions, fitted curves of which are indicated by solid lines. With decoupled nondegerate TPA signals in the time domain, a 2D contour plotting is generated in Figure 3(c) for visualization purpose. To verify the above interpretation, we perform a direct measurement of cross-correlation between pump and probe pulses, which is determined by pulse widths of our laser system. With a beta barium borate (BBO) crystal, time-dependent sum frequency generation (SFG) of a 810 nm pulse from the Ti: sapphire oscillator and a 1525 nm pulse from the optical parametric oscillator is recorded, as shown in Figure 3(d). It should be noticed that pump and probe pulses for monolayer WS_2 measurements are from the same Ti: sapphire oscillator and optical parametric oscillator (see Supporting Information). According to Gaussian fitting of the black line, FWHM of cross-correlation of pump and probe pulses turns out to be about 227 fs. In Figure 3(e), we plot FWHM (blue triangles) and minimal values (red diamonds) of fitted curves in Figure 3(b) as a function of 776 nm pump irradiance. Observed FWHM of nondegenerate TPA signals, fluctuating between 200 fs and 250 fs, are satisfactorily consistent with SFG cross-correlation observation. What's more, minimal values of nondegenerate TPA signals are linearly decreasing with pump irradiances. At this point, we have completely decoupled

nondegenerate TPA signals from degenerate TPA signals in monolayer WS_2.

To derive degenerate and nondegenerate TPA coefficients of the monolayer WS_2, degenerate and nondegenerate TPA induced by the pump and probe beams for a thin sample can be described as,[49]

$$\begin{aligned} \frac{\partial I_p}{\partial z} &= -\beta(\omega_p){I_p}^2 - 2\beta(\omega_p;\omega_e)I_pI_e, \\ \frac{\partial I_e}{\partial z} &= -\beta(\omega_e){I_e}^2 - 2\beta(\omega_e;\omega_p)I_eI_p, \end{aligned} \tag{3}$$

I_p and I_e are the pump and probe irradiance, respectively. Since we have fully decoupled the nondegenerate TPA signal from transient absorption signals induced by degenerate TPA, equations of pump and probe beams can be simplified to,

$$\begin{aligned} \frac{\partial I_p}{\partial z} &= -\beta(\omega_p){I_p}^2, \\ \frac{\partial I_e}{\partial z} &= -2\beta(\omega_e;\omega_p)I_eI_p. \end{aligned} \tag{4}$$

The solutions are,

$$\begin{aligned} I_p(z) &= \frac{I_p(0)}{1+\beta(\omega_p)I_p(0)z}, \\ I_e(z) &= I_e(0)e^{-2\beta(\omega_e;\omega_p)I_pz}. \end{aligned} \tag{5}$$

Thus absorptances of pump and probe irradiances become

$$\begin{aligned} \frac{I_p(0)-I_p(z)}{I_p(0)} &= \frac{\beta(\omega_p)I_p(0)z}{1+\beta(\omega_p)I_p(0)z} \approx \beta(\omega_p)I_p(0)z, \\ \frac{I_e(0)-I_e(z)}{I_e(0)} &= 1-e^{-2\beta(\omega_e;\omega_p)I_pz}, \end{aligned} \tag{6}$$

where the approximation is made based on the fact that $\frac{I_p(0)-I_p(z)}{I_p(0)} \ll 1$ and $\beta(\omega_p)I_p(0)z \ll 1$. Hence, degenerate and nondegenerate TPA coefficients account for absorptances of pump and probe irradiances, respectively. Absorptances of pump irradiances induced by degenerate TPA as well as degenerate TPA coefficients can be immediately obtained by scaling injected carrier densities via degenerate TPA with that via OPA, since electron transitions via both

OPA and TPA processes have the same initial and final states. Meanwhile, nondegenerate TPA coefficients can be directly calculated by decoupled nondegenerate TPA signals before 0 fs, that are absorptances of probe irradiances. Details of our calculations are presented in Supporting Information.

In Figure 3(f), under non-resonant pumping conditions, calculated degenerate and nondegenerate TPA coefficients of monolayer WS_2 are plotted as a function of 776 nm pump irradiance in black squares and red circles, respectively. Both of them indicate linearly decreasing trends with increasing pump irradiances. From the sub-linear trend of carrier saturation observed in Figure 2(e), we attribute decreasing TPA coefficients of monolayer WS_2 to band-filling effects. Estimated by intercepts of linear fittings (solid lines) in Figure 3(f) when pump irradiance is zero, intrinsic magnitudes of degenerate and nondegenerate TPA coefficients in monolayer WS_2 are about 100 ± 10 cm/GW and 250 ± 30 cm/GW, respectively. Nondegenerate TPA coefficient is about a factor of 2.5 larger than degenerate TPA coefficient, when $1s$ excitonic level serves as a real intermediate state for nondegenerate TPA.

To investigate excitonic resonance enhancement of TPA, we apply resonant pumping conditions for a monolayer $MoSe_2$ sample and perform similar measurements. In the meantime, a trilayer $MoSe_2$ sample is studied for comparison. The PL spectra of these two samples fabricated on BK7 glass substrates are presented in Figure 4(a). The PL peaks of monolayer and trilayer $MoSe_2$ are at 792 nm and 812 nm, respectively. Intensity of trilayer $MoSe_2$ PL is about two-order of magnitude weaker than that of monolayer, agreeing well with previous reports.[50,51] In pump-probe measurements, we choose 790 nm pulse as the probe, 750 nm pulse as the OPA pump and 1500 nm pulse as the TPA pump (see Supporting Information). Photon energy of 750 nm pump, that is equivalent to two photons of 1500 nm pump, is higher by 84 meV than monolayer $MoSe_2$ optical band gap $E_o = 1.57$ eV but much less than electronic band gap,[21,52,53] so that electron transitions fall into excitonic levels. According to observations of excitonic levels in monolayer $MoSe_2$ at 4 K by Wang et al.,[52] $2p$ level of

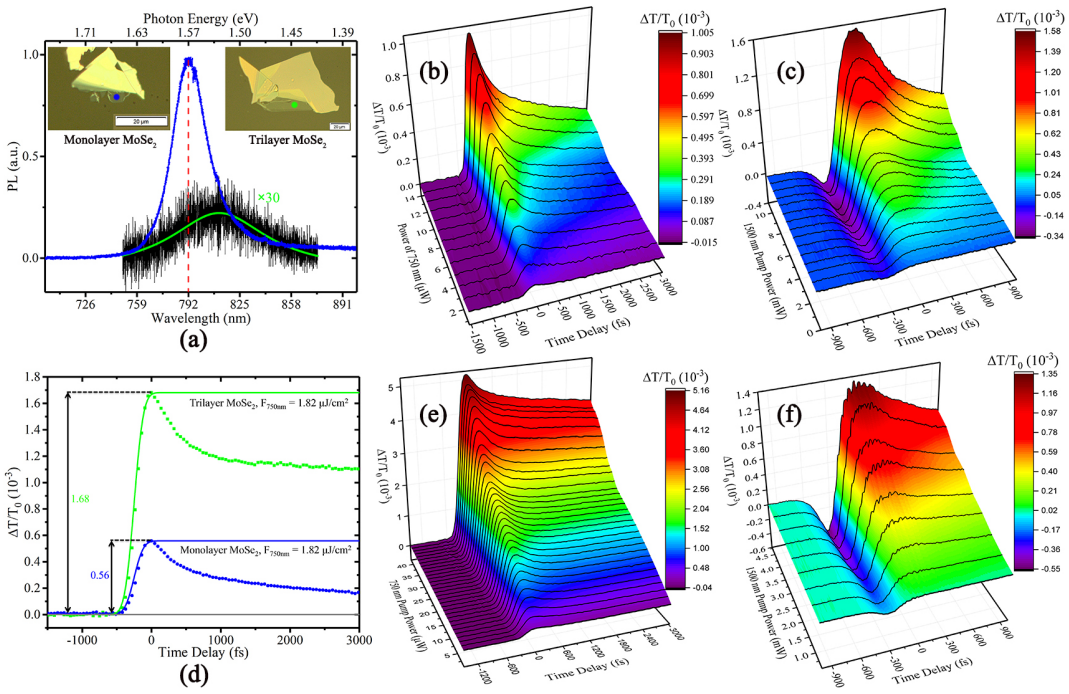

Figure 4: (a) PL spectra of monolayer and trilayer $MoSe_2$ samples denoted by blue and green curves, respectively. The green curve is a lorentzian fitting of original data in black. Insets are optical microscope images of samples, where blue and green dots are laser focusing positions. (b) and (c) are OPA and TPA measurement results of monolayer $MoSe_2$, respectively. (d) Temporal scans of differential transmission signals in monolayer (blue circles) and trilayer (green squares) $MoSe_2$ under equal 750 nm pump fluence of 1.82 $\mu J/cm^2$. The magnitude of differential transmission signal at 0 fs in trilayer $MoSe_2$ is three times of that in monolayer. Blue and green lines are a temporal integral of Gaussian pulses with FWHM of 300 fs. (e) and (f) are OPA and TPA measurement results of trilayer $MoSe_2$, respectively.

A exciton was not only higher by 180 meV than $1s$ level of A exciton, but also overlapping with $1s$ level of B exciton. It should be noticed that our measurements are performed at room temperature (300 K). Since all excitonic resonances in TMD semiconducting monolayers would broaden as temperature increases from 4 K to 300 K, it is possible that the tails of $1s$ states of B exciton and $2p$ states of A exciton fall into our laser wavelengths. Since $1s$ states of B exciton are parity forbidden for a TPA process, degenerate TPA in monolayer $MoSe_2$ is then realized by resonantly exciting electrons from valence band to $2p$ states of A exciton.

We first investigate monolayer $MoSe_2$ by measuring temporal dynamics of carriers under different 750 nm and 1500 nm pump powers, corresponding results of which are shown in

Figure 4(b) and (c), respectively. Subsequently, we carry out the same measurements in trilayer $MoSe_2$, results of which for OPA and TPA are illustrated in Figure 4(e) and (f), respectively. In Figure 4(d), we compare temporal dynamics of probe differential transmission in monolayer and trilayer $MoSe_2$, taken under equal 750 nm pump fluence of 1.82 μJ/cm^2. Solid blue and green lines are fittings for rising parts with Gaussian integral, and obtained FWHM of cross-correlation of pump and probe pulses in both cases are about 300 fs. In addition, the magnitude of probe differential transmission at 0 fs in trilayer $MoSe_2$ are exactly three times of that in monolayer, as illustrated by black double-arrows, which further confirm relative thicknesses of these two samples.

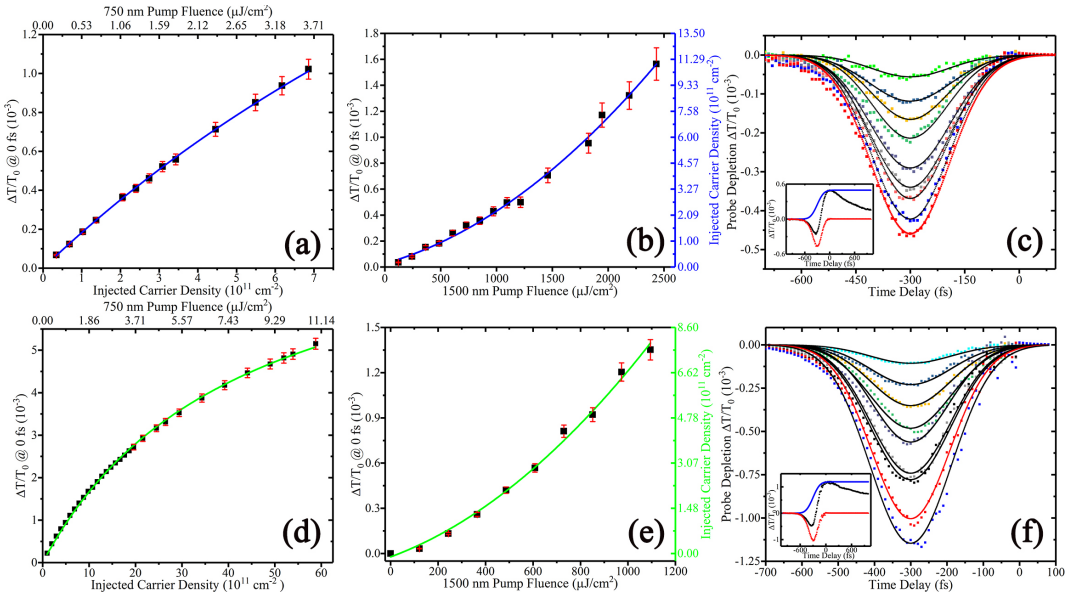

Figure 5: Differential transmission signals at 0 fs in monolayer $MoSe_2$ (a) as a function of injected carrier density in OPA measurements and (b) as a function of 1500 nm pump fluence in TPA measurements, where blue lines are sublinear and quadratic fittings, respectively. (c) Decoupled nondegenerate TPA signals in monolayer $MoSe_2$ when 1500 nm pump powers increase from 0.53 mW (top) to 4.80 mW (bottom). Inset is an example of decoupling process when 1500 nm pump power is 4.80 mW. In a manner of the same style, corresponding results of trilayer $MoSe_2$ are illustrated in (d), (e) and (f). In (f), 1500 nm pump powers are from 0.53 mW (top) to 4.80 mW (bottom). Inset is an example of decoupling process when 1500 nm pump power is 4.26 mW.

Next, we process results of monolayer and trilayer $MoSe_2$ similarly as we have discussed above for monolayer WS_2. Pump fluence dependences of OPA, degenerate TPA and nonde-

generate TPA in monolayer $MoSe_2$ are listed in Figure 5(a), (b) and (c), respectively. From injected carrier density dependence of probe differential transmission at 0 fs via OPA of monolayer $MoSe_2$ in Figure 5(a), carrier saturation parameters of $A = 0.005$ and $N_0 = 2.4 \times 10^{12}$ cm^{-2} are obtained by fitting black squares with Equation (2). For pump fluence dependence of probe differential transmission at 0 fs via TPA of monolayer $MoSe_2$ in Figure 5(b), a quadratic fitting matches well with black squares. As shown in Figure 5(c), decoupled nondegenerate TPA signals when 1500 nm pump powers increase from 0.53 mW (top) to 4.80 mW (bottom) are fitted with negative Gaussian functions, and fitted curves are in solid lines. Inset is an example of decoupling process when 1500 nm pump power is 4.80 mW, pump irradiance of which is 5.63 GW/cm^2. In a manner of the same style, corresponding results for trilayer $MoSe_2$ are listed in Figure 5(d)-(f). Obtained carrier saturation parameters in trilayer $MoSe_2$ are $A = 0.009$ and $N_0 = 4.3 \times 10^{12}$ cm^{-2}. In Figure 5(f), decoupled nondegenerate TPA signals when 1500 nm pump powers increase from 0.53 mW (top) to 4.80 mW (bottom) are fitted with negative Gaussian functions, and fitted curves are in solid lines. Inset is an example of decoupling process when 1500 nm pump power is 4.26 mW, pump irradiance of which is 5.00 GW/cm^2.

Based on the results in Figure 5, we are able to calculate the degenerate and nondegenerate TPA coefficients under different pump irradiances (see Supporting Information). In monolayer $MoSe_2$, probe depletions at -300 fs, depicted in red diamonds and fitted in solid red line in Figure 6(a), present a linear dependence of pump irradiance. Fitted FWHM of pump-probe cross-correlation from probe depletion curves of Figure 5(c), denoted by blue triangles in Figure 6(a), remain a horizontal trend, which strongly validates the quality of our experimental measurements and temporally decoupling model.

Calculated degenerate and nondegenerate TPA coefficients of monolayer $MoSe_2$ under different 1500 nm pump irradiances, are denoted by black squares and red circles, respectively, in Figure 6(b). Different from monolayer WS_2, considerably large degenerate TPA coefficients of monolayer $MoSe_2$ under resonant pumping conditions, not only emerge when

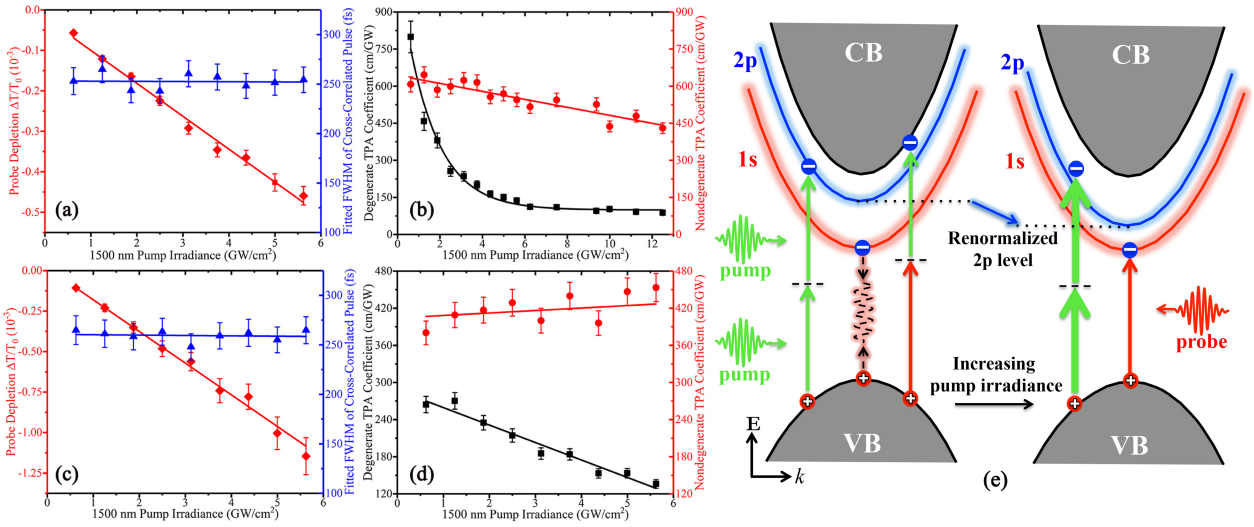

Figure 6: (a) Probe depletions at -300 fs (red diamonds) in monolayer $MoSe_2$ induced by nondegenerate TPA as a function of 1500 nm pump irradiance. Blue triangles are FWHM of fitted curves of nondegenerate TPA signals. Solid lines are linear fittings. (b) Degenerate TPA coefficients (black squares) and nondegenerate TPA coefficients (red circles) as a function of 1500 pump irradiance. Solid black and red lines are an exponential fitting and a linear fitting, respectively. Corresponding results in trilayer $MoSe_2$ are illustrated in (c) and (d) in a similar style. (e) Red-shift of $2p$ excitonic level induced by band renormalization effect when increasing pump irradiance, rapidly switches off excitonic resonance of degenerate TPA in monolayer $MoSe_2$.

1500 nm pump irradiances are below 2 GW/cm^2, but also present a rapidly decreasing trend. The solid black line in Figure 6(b) is an exponential fitting. To interpret this result of monolayer $MoSe_2$, we can bring up a hypothesis by the following discussions. First of all, higher order nonlinear optical effects, such as three-photon absorption, is less likely to affect our measurements of monolayer $MoSe_2$. Three-photon absorption would fall into continuum states of monolayer $MoSe_2$ instead of excitonic states. More importantly, their contributions to total carrier density are expected to be at least three orders of magnitude smaller than TPA, due to the nonlinear optical susceptibility scaling rule. Secondly, according to several recent observations,[3,4] excitonic levels of TMD monolayers significantly deviate from 2D Rydberg model for a hydrogen atom. As a result, exact positions of excitonic levels as well as intrinsic values of exciton binding energy are still an un-settled issue. Different screening effects of sample dielectric environment, reshaping the electron-hole interaction

potentials, might be a possible reason. We notice in a very recent work that giant binding energy modulation of exciton complexes has been realized by varying dielectric medium around monolayer $MoSe_2$.[54] About 60 % reduction of A exciton binding energy in monolayer $MoSe_2$ was observed.[54] Noticing that our monolayer $MoSe_2$ sample was fabricated on a 0.48 mm thick BK7 glass substrate instead of a SiO_2/Si substrate employed by Wang et al.,[52] a different $1s$-$2p$ separation can be reasonably expected. Last but not the least, comparing with linearly decreasing trends of degenerate TPA coefficients in monolayer WS_2 and trilayer $MoSe_2$, observed exponentially decreasing trend of degenerate TPA coefficients in monolayer $MoSe_2$ under resonant pumping, indicates the excitonic resonance of $2p$ states was turned off when increasing pump irradiance. This phenomenon can be possibly attributed to the red-shift of $2p$ states induced by band renormalization under increasing pump irradiances, as illustrated by the schematic diagram in Figure 6(e). When 1500 nm pump irradiance is above 4 GW/cm^2, absorption saturation caused by band-filling effect will dominate and lead to a linearly decreasing trend of degenerate TPA coefficient, which is similar to the case of monolayer WS_2. Therefore, based on these discussions, the observed exponential decrease of degenerate TPA coefficients in monolayer $MoSe_2$ is possibly induced by the interplay between band renormalization effect and band-filling effect. It is also interesting that when 1500 nm pump irradiance gets higher than 6 GW/cm^2, degenerate TPA coefficients of monolayer $MoSe_2$ drop to a magnitude of about 80 cm/GW, which is almost equal to the degenerate TPA coefficients observed in monolayer WS_2 in Figure 3(f). Overall, under resonant pumping of $2p$ excitonic states, degenerate TPA coefficient of monolayer $MoSe_2$ is enhanced by at least one order of magnitude, and by simply increasing pump irradiance, one can actively control degenerate TPA coefficient as well as fine structures of excitonic levels. Thus it is confirmed that our time-resolved technique can effectively initiate and sensitively monitor dynamical change of $2p$ excitonic levels via degenerate TPA in monolayer $MoSe_2$, demonstrating its potential for actively controlling nonlinear excitonic dynamics in 2D semiconducting monolayers.

Furthermore, final state of nondegenerate TPA in monolayer $MoSe_2$ falls into conduction band and non-resonant pumping conditions are applied, so that band renormalization effect plays a minor role than band-filling effect to decrease nondegenerate TPA coefficient. As a result, nondegenerate TPA coefficients still maintain a linearly decreasing trend, as shown by red circles in Figure 6(b). Intrinsic nondegenerate TPA coefficient of monolayer $MoSe_2$ is about 650 $\pm$ 50 cm/GW, which is estimated by the intercept of the linearly fitting line. Magnitude of nondegenerate TPA coefficients are larger than degenerate TPA coefficients by a factor of about 5 when 1500 nm pump irradiance is above 6 GW/cm^2. For comparison, according to results in Figure 6(c) and (d), degenerate TPA coefficients of trilayer $MoSe_2$ present a linearly decreasing trend instead of exponentially decreasing trend as observed in monolayer. This is reasonable for trilayer $MoSe_2$ because the pump is no longer resonant with the direct exciton transition. When 1500 nm pump irradiance is below 1 GW/cm^2, degenerate TPA coefficient is estimated to be about 260 cm/GW, which is $\frac{1}{3}$ of monolayer magnitude. Above 6 GW/cm^2, degenerate as well as nondegenerate TPA coefficients of trilayer are almost equal to monolayer values. These results suggest that carrier injection via TPA in monolayer and trilayer $MoSe_2$ tend to reach comparable efficiencies when pump irradiances are around 6 GW/cm^2.

To justify the negligible contribution of nondegenerate TPA to injected carrier density, in Supporting Information we calculate injected carrier densities via nondegenerate TPA for all the three samples we have studied. Although nondegenerate and degenerate TPA are synchronously induced in our experiments, our calculations indicate that injected carrier density via nondegenerate TPA is about two-order of magnitude smaller than that via degenerate TPA. We notice that degenerate and nondegenerate TPA coefficients of monolayer WS_2 and $MoSe_2$ we have observed, are considerably large. For instance, degenerate TPA coefficients of monolayer $MoSe_2$ are about two-order of magnitude higher than traditional semiconductors, such as Si: 2 cm/GW,[55] ZnO: 5 cm/GW[56] and GaAs: 26 cm/GW.[57] Facilitated by their large TPA coefficients, one could expect that TMD monolayers with band gaps in

visible region could be utilized for subband photodetection in the infrared region. We also notice that degenerate TPA coefficient of 525 ± 205 cm/GW in 1-3 layer CVD WS_2 has been reported in degenerate TPA Z-scan measurements by Zhang et al.[17] The degenerate TPA coefficients measured in exfoliated monolayer WS_2 with femtosecond laser pump-probe technique in this paper are on the same order of magnitude and reasonably consistent.

4. Conclusion

In conclusion, utilizing femtosecond laser pump-probe, we have realized simultaneous observations of degenerate and nondegenerate TPA processes in WS_2 and $MoSe_2$ monolayers, that are synchronously induced and recorded by temporally scanning a probe pulse across a pump pulse. A decoupling model has been established to fully separate co-existing positive and negative components of differential transmission signals in the first 500 fs, enabling us to extract both degenerate and nondegenerate TPA coefficients from only one temporal scan. Calculated degenerate and nondegenerate TPA coefficients of monolayer WS_2 under non-resonant pumping are 100 ± 10 cm/GW and 250 ± 25 cm/GW, respectively, which are about two orders of magnitude higher than that of conventional semiconductors. In addition, they both monotonically decrease as a function of pump irradiance due to band-filling effects. However, under resonant pumping of $2p$ excitonic states in monolayer $MoSe_2$, although nondegenerate TPA coefficients still linearly decrease with an intrinsic magnitude of 650 ± 50 cm/GW, degenerate TPA coefficients exponentially decrease from 800 to 80 cm/GW when pump irradiances increase from 0.6 to 12.5 GW/cm^2. By comparison measurements of a trilayer $MoSe_2$, such exponential dependence on pump irradiance is attributed to the interplay between band-renormalization and band-filling effects. Overall, our measurements suggest that excitonic resonance can not only enhance the degenerate TPA coefficient of 2D semiconducting monolayers by at least one order of magnitude, but also be readily switched on and off through simply adjusting pump irradiance. Therefore, our results could pave

the way toward sensitive measurement of TPA coefficients and active control of nonlinear excitonic dynamics via TPA in 2D semiconducting monolayers.

Acknowledgement

This work was supported by National Natural Science Foundation of China (Nos. 61704024, 61475035, 11734005 and 11374161), Natural Science Foundation of Jiangsu Province (No. BK20170696), Primary Research and Development Plan of Jiangsu Province (Nos. BE2016177 and BE2016756), National Key Research and Development Plan of China (Nos. 2017YFA0700500 and 2018YFA0209101), and National Science Foundation of USA under Award No. DMR-1505852. Q. C. gratefully acknowledges the support of Southeast University through Zhishan Young Scholar Fund.

References

(1) K. F. Mak, C. Lee, J. Hone, J. Shan, T. F. Heinz, *Phys. Rev. Lett.* **2010**, *105*, 136805.

(2) A. Splendiani, L. Sun, Y. Zhang, T. Li, J. Kim, C.-Y. Chim, G. Galli, F. Wang, *Nano Lett.* **2010**, *10*, 1271.

(3) A. Chernikov, T. C. Berkelbach, H. M. Hill, A. Rigosi, Y. Li, O. B. Aslan, D. R. Reichman, M. S. Hybertsen, T. F. Heinz, *Phys. Rev. Lett.* **2014**, *113*, 076802.

(4) K. He, N. Kumar, L. Zhao, Z. Wang, K. F. Mak, H. Zhao, J. Shan, *Phys. Rev. Lett.* **2014**, *113*, 026803.

(5) M. Bernardi, M. Palummo, J. C. Grossman, *Nano Lett.* **2013**, *13*, 3664.

(6) M.-L. Tsai, S.-H. Su, J.-K. Chang, D.-S. Tsai, C.-H. Chen, C.-I. Wu, L.-J. Li, L.-J. Chen, J.-H. He, *ACS Nano* **2014**, *8*, 8317.

(7) Y. Ye, Z. J. Wong, X. Lu, X. Ni, H. Zhu, X. Chen, Y. Wang, X. Zhang, *Nat. Photonics* **2015**, *9*, 733.

(8) Y. Li, J. Zhang, D. Huang, H. Sun, F. Fan, J. Feng, Z. Wang, C. Z. Ning, *Nat. Nanotechnol.* **2017**, *12*, 987.

(9) D. Chimene, D. L. Alge, A. K. Gaharwar, *Adv. Mater.* **2015**, *27*, 7261.

(10) M. Pumera, A. H. Loo, *TrAC, Trends Anal. Chem.* **2014**, *61*, 49.

(11) N. Kumar, S. Najmaei, Q. Cui, F. Ceballos, P. M. Ajayan, J. Lou, H. Zhao, *Phys. Rev. B* **2013**, *87*, 161403.

(12) Q. Cui, R. A. Muniz, J. E. Sipe, H. Zhao, *Phys. Rev. B* **2017**, *95*, 165406.

(13) H. Yang, X. Feng, Q. Wang, H. Huang, W. Chen, A. T. S. Wee, W. Ji, *Nano Lett.* **2011**, *11*, 2622.

(14) K. Wang, J. Wang, J. Fan, M. Lotya, A. O'Neill, D. Fox, Y. Feng, X. Zhang, B. Jiang, Q. Zhao, H. Zhang, J. N. Coleman, L. Zhang, W. J. Blau, *ACS Nano* **2013**, *7*, 9260.

(15) Z. Luo, Y. Li, M. Zhong, Y. Huang, X. Wan, J. Peng, J. Weng, *Photonics Res.* **2015**, *3*, A79.

(16) R. I. Woodward, R. C. T. Howe, T. H. Runcorn, G. Hu, F. Torrisi, E. J. R. Kelleher, T. Hasan, *Opt. Express* **2015**, *23*, 20051.

(17) S. Zhang, N. Dong, N. McEvoy, M. O'Brien, S. Winters, N. C. Berner, C. Yim, Y. Li, X. Zhang, Z. Chen, L. Zhang, G. S. Duesberg, J. Wang, *ACS Nano* **2015**, *9*, 7142.

(18) X. Zheng, Y. Zhang, R. Chen, X. Cheng, Z. Xu, T. Jiang, *Opt. Express* **2015**, *23*, 15616.

(19) N. Dong, Y. Li, S. Zhang, N. McEvoy, R. Gatensby, G. S. Duesberg, J. Wang, *ACS Photonics* **2018**, *5*, 1558.

(20) G. Wang, X. Marie, I. Gerber, T. Amand, D. Lagarde, L. Bouet, M. Vidal, A. Balocchi, B. Urbaszek, *Phys. Rev. Lett.* **2015**, *114*, 097403.

(21) M. M. Ugeda, A. J. Bradley, S.-F. Shi, H. Felipe, Y. Zhang, D. Y. Qiu, W. Ruan, S.-K. Mo, Z. Hussain, Z.-X. Shen, F. Wang, S. G. Louie, M. F. Crommie, *Nat. Mater.* **2014**, *13*, 1091.

(22) P. D. Cunningham, A. T. Hanbicki, K. M. McCreary, B. T. Jonker, *ACS Nano* **2017**, *11*, 12601.

(23) F. Zhou, J. Wei, *Opt. Lett.* **2017**, *42*, 3113.

(24) T. Jiang, D. Huang, J. Cheng, X. Fan, Z. Zhang, Y. Shan, Y. Yi, Y. Dai, L. Shi, K. Liu, C. Zeng, J. Zi, J. E. Sipe, Y.-R. Shen, W.-T. Liu, S. Wu, *Nat. Photonics* **2017**, *12*, 430.

(25) G. Soavi, G. Wang, H. Rostami, D. G. Purdie, D. De Fazio, T. Ma, B. Luo, J. Wang, A. K. Ott, D. Yoon, S. A. Bourelle, J. E. Muench, I. Goykhman, S. Dal Conte, M. Celebrano, A. Tomadin, M. Polini, G. Cerullo, A. C. Ferrari, *Nat. Nanotechnol.* **2018**, *13*, 583.

(26) Q. Cui, H. Zhao, *ACS Nano* **2015**, *9*, 3935.

(27) K. Hao, L. Xu, P. Nagler, A. Singh, K. Tran, C. K. Dass, C. Schuller, T. Korn, X. Li, G. Moody, *Nano Lett.* **2016**, *16*, 5109.

(28) M. Titze, B. Li, X. Zhang, P. M. Ajayan, H. Li, *Phys. Rev. Mater.* **2018**, *2*, 054001.

(29) S.-Y. Hong, J. I. Dadap, N. Petrone, P.-C. Yeh, J. Hone, R. M. Osgood Jr, *Phys. Rev. X* **2013**, *3*, 021014.

(30) N. Kumar, J. Kumar, C. Gerstenkorn, R. Wang, H.-Y. Chiu, A. L. Smirl, H. Zhao, *Phys. Rev. B* **2013**, *87*, 121406.

(31) R. Wang, H.-C. Chien, J. Kumar, N. Kumar, H.-Y. Chiu, H. Zhao, *ACS Appl. Mater. Interfaces* **2013**, *6*, 314.

(32) M. J. Rodrigues, C. J. de Matos, Y. W. Ho, H. Peixoto, R. E. de Oliveira, H.-Y. Wu, A. H. C. Neto, J. Viana-Gomes, *Adv. Mater.* **2016**, *28*, 10693.

(33) N. Youngblood, R. Peng, A. Nemilentsau, T. Low, M. Li, *ACS Photonics* **2016**, *4*, 8.

(34) M. Sheik-Bahae, A. A. Said, T.-H. Wei, D. J. Hagan, E. W. Van Stryland, *IEEE J. Quantum Electron.* **1990**, *26*, 760.

(35) M. Sheik-Bahae, J. Wang, R. DeSalvo, D. J. Hagan, E. W. Van Stryland, *Opt. Lett.* **1992**, *17*, 258.

(36) J. Wang, M. Sheik-Bahae, A. A. Said, D. J. Hagan, E. W. Van Stryland, *J. Opt. Soc. Am. B* **1994**, *11*, 1009.

(37) L. A. Padilha, J. Fu, D. J. Hagan, E. W. Van Stryland, C. L. Cesar, L. C. Barbosa, C. H. B. Cruz, D. Buso, A. Martucci, *Phys. Rev. B* **2007**, *75*, 075325.

(38) C. M. Cirloganu, L. A. Padilha, D. A. Fishman, S. Webster, D. J. Hagan, E. W. Van Stryland, *Opt. Express* **2011**, *19*, 22951.

(39) D. A. Fishman, C. M. Cirloganu, S. Webster, L. A. Padilha, M. Monroe, D. J. Hagan, E. W. Van Stryland, *Nat. Photonics* **2011**, *5*, 561.

(40) M. Reichert, A. L. Smirl, G. Salamo, D. J. Hagan, E. W. Van Stryland, *Phys. Rev. Lett.* **2016**, *117*, 073602.

(41) W. Zhao, Z. Ghorannevis, L. Chu, M. Toh, C. Kloc, P.-H. Tan, G. Eda, *ACS Nano* **2012**, *7*, 791.

(42) J. He, D. He, Y. Wang, Q. Cui, F. Ceballos, H. Zhao, *Nanoscale* **2015**, *7*, 9526.

(43) N. Kumar, B. A. Ruzicka, N. Butch, P. Syers, K. Kirshenbaum, J. Paglione, H. Zhao, *Phys. Rev. B* **2011**, *83*, 235306.

(44) F. Ceballos, Q. Cui, M. Z. Bellus, H. Zhao *Nanoscale* **2016**, *8*, 11681.

(45) Y. Li, A. Chernikov, X. Zhang, A. Rigosi, H. M. Hill, A. M. van der Zande, D. A. Chenet, E.-M. Shih, J. Hone, T. F. Heinz, *Phys. Rev. B* **2014**, *90*, 205422.

(46) K. Xu, Z. Wang, X. Du, M. Safdar, C. Jiang, J. He, *Nanotechnology* **2013**, *24*, 465705.

(47) X. Huang, Z. Zeng, H. Zhang, *Chem. Soc. Rev.* **2013**, *42*, 1934.

(48) R. W. Boyd, *Nonlinear Optics*, San Diego, USA: Academic Press, **2008**.

(49) B. V. Olson, M. P. Gehlsen, T. F. Boggess, *Opt. Commun.* **2013**, *304*, 54.

(50) P. Tonndorf, R. Schmidt, P. Böttger, X. Zhang, J. Börner, A. Liebig, M. Albrecht, C. Kloc, O. Gordan, D. R. T. Zahn, S. M. de Vasconcellos, R. Bratschitsch, *Opt. Express* **2013**, *21*, 4908.

(51) S. Tongay, J. Suh, C. Ataca, W. Fan, A. Luce, J. S. Kang, J. Liu, C. Ko, R. Raghunathanan, J. Zhou, F. Ogletree, J. Li, J. C. Grossman, J. Wu, *Sci. Rep.* **2013**, *3*, 2657.

(52) G. Wang, I. Gerber, L. Bouet, D. Lagarde, A. Balocchi, M. Vidal, T. Amand, X. Marie, B. Urbaszek, *2D Mater.* **2015**, *2*, 045005.

(53) S. Tongay, J. Zhou, C. Ataca, K. Lo, T. S. Matthews, J. Li, J. C. Grossman, J. Wu, *Nano Lett.* **2012**, *12*, 5576.

(54) G. Gupta, S. Kallatt, K. Majumdar, *Phys. Rev. B* **2017**, *96*, 081403.

(55) A. D. Bristow, N. Rotenberg, H. M. van Driel, *Appl. Phys. Lett.* **2007**, *90*, 191104.

(56) E. W. Van Stryland, M. A. Woodall, H. Vanherzeele, M. J. Soileau, *Opt. Lett.* **1985**, *10*, 490.

(57) A. A. Said, M. Sheik-Bahae, D. J. Hagan, T. H. Wei, J. Wang, J. Young, E. W. Van Stryland, *J. Opt. Soc. Am. B* **1992**, *9*, 405.